A Description of the 64-Meter Antenna Elevation Drive Gears and Their Strange Wear

H. McGinness
Ground Antennas and Facilities Engineering Section

The elevation drive gears are described and their wear is compared to the wear of other antenna drive gears. The comparison is perplexing and satisfying explanations have not yet been made.

I. Introduction

The 64-m antenna elevation axis drive is executed by torquing two bull gears, concentric to the elevation axis, with the output pinions of four gear boxes. These gear boxes have functioned well during the 18 and 11 years, respectively, that the DSS 14, and the DSS 43 and DSS 63 antennas have been in service. A strange wear pattern gradually developed on the bull gears and driving pinions of all three antennas. These patterns were well developed after 8 years and apparently are intensifying in all instances.

II. Description of the Drives and the Gear Wear

The gear boxes are mounted so as to allow the output pinions to self-align to the bull gears. Figures 1 and 2 show how the gear boxes are pivoted with a ball joint at one end such that the tangential load on the output pinion passes through the ball joint. The other end of each gear box is supported by one horizontal and two vertical spring-loaded struts. The gear box contains a reaction roller, mounted opposite the pinion, which rolls on the inside of the bull-gear ring and equilibrates the separation force between the bull gear and pinion. The ball-joint pivot, together with the three spring-loaded struts, allows the pinion to execute small angles of roll, pitch, and yaw which may be required to maintain near-perfect mesh between the pinion and the bull gear, as the bull gear deviates from perfection. A detailed description of this gear-box suspension is given in Ref. 1.

Each gear box has two input shafts which are geared to a common shaft. One input shaft has a constant torque applied in a direction opposite to that of its corresponding shaft on the other gear box, which meshes with the same bull gear. The two opposing, countertorquing shafts eliminate backlash from the gear system. The second input shaft is the driving input and its torque has the proper direction and magnitude to equilibrate the antenna axis torque caused by wind or imbalance. A schematic of this torquing system is shown in Fig. 3. Whenever the wind torque is below a certain value, the countertorques are greater than the driving torques and the two output pinions bear against opposite faces of the bull-gear teeth. This is designated as Case I loading. It is estimated that this Case I loading condition prevails more than 97% of the time.

When the wind torque is above a certain value, the driving torques are greater than the countertorques. This is designated as Case II loading. One driving torque direction is always the same as its countertorque direction, whereas the other driving torque is always opposite to its countertorque direction; hence, for Case II loading, one of the output pinions bears against the bull-gear tooth face opposite to that for the Case I loading. For either Case I or Case II loading one of the output

pinions has its load increased from its countertorque loading whenever the wind blows, and the amount of the increase is proportional to the square of the wind speed and the wind torque coefficient. Therefore, the load range on one of the output pinions is from the countertorque value to approximately four times that value at a wind speed of 22.35 m/sec (50 MPH). Wind records at DSS 14 [Ref.9] show that the wind exceeds 4.47 m/sec (10 MPH) only *44%* of the time; therefore, for *56%* of the time the countertorque loading of a *68877* N (15485 lb) tangential force is barely exceeded. The wind loading may be obtained from Ref. 2.

The strange wear pattern, which is described below, exists on all bull-gear teeth which are exposed to the driving pinions. It is believed that if the wear pattern were caused by the high loads from infrequent high winds, the patterns would exist only on relatively few teeth, namely, those in mesh during the few predominant antenna orientations of high loading. Therefore, the conclusion is that the wear pattern is caused primarily by the constant but much smaller forces from the countertorquing pinions. The sides of the teeth subjected to this constant countertorquing are shown in Fig. 4.

The bull-gear wear pattern is shown in Figs. 5, 6, and 7. It consists of a series of diagonal waves (with peak-to-valley amplitudes judged to be as much as 0.50 mm) terminating at the pitch line of each gear tooth. The direction of the diagonals is sometimes reversed across the pitch line. The phenomenon has been described by several gear consultants as a plastic flow condition. Several references allude to plastic flow, for example, page 506 of Ref. 3 states,

> With the softer and more plastic materials tested, a definite plastic flow of the surface material occurs, even though particles are not sheared out of the surface. Sometimes this plastic flow develops into a series of waves on the surface. With the introduction of sliding between the two surfaces in generally rolling contact, this corrugation effect is increased greatly. . . . Some borderline cases may show up with inadequate lubrication that would not exist under more favorable conditions of lubrication, notably the plastic flow of the surface with the development of hollows and ridges.

Page 520 of Ref. 3 states, "On the softer steels under 200 Brinell hardness number, for example, corrugations or waves are developed on the surface, particularly if sliding action is present, under relatively light loads." Page 16 of Ref. 4 states,

> Plastic flow is the cold working of the tooth surfaces, caused by high contact stresses and the rolling and sliding action of the mesh. It is a surface deformation resulting from the yielding of the surface and subsurface material. It is usually associated with the softer gear materials, although it often occurs in heavily loaded case hardened and through hardened gears.

This same reference discusses the plastic flow phenomena termed "rippling" and "ridging" and associates them with high contact stresses. Photographs of rippling and ridging examples are shown in Ref. 4.

None of the above references quantitatively relate plastic flow to the ratio of contact stress to material yield stress. If a gear designer assiduously evaluates all load and stress conditions and selects a material having yield strengths above any possible stress value, he might expect that plastic flow would be prevented. Since plastic flow sometimes occurs in spite of such considerations, the explanation probably lies in a possible reduction of the material yield strength under the cyclical loading which is, of course, the nature of gear-tooth loading. Since plastic flow does not occur most of the time when gears are designed in accordance with rules which ensure that maximum contact stresses are sufficiently below the "nominal yield strength" of the material, it might be that certain alloys at certain hardnesses require that, in order to prevent plastic flow, the maximum contact stresses must be below the "nominal yield strength" by a much greater amount than is usually required. The "nominal yield strength" as used above means the yield strength as determined by a monotonically increasing load. The phenomenon of material strain softening as described in Refs. 5 and 6 is a weakening effect that is much greater for some materials than for others. The curve of Fig. 11 indicates that for 4142 steel at a Brinell hardness of *380*, the yield strength after cyclical loading is approximately 50% of the monotonic yield strength. This 4142 alloy is approximately the same as the elevation bull-gear material 4140 although the bull-gear hardness range was originally about 245 to 285 Brinell.

The elevation bull-gear and pinion specifications can be obtained, respectively, from the JPL drawings 9436786 and 9435055. Some of the specifications are listed in Table 1.

The bull gears and pinions are exposed to debris which is transported by wind. The use of a sticky lubricant was considered inappropriate because of the debris it would collect. The dry lubricant which has been employed comes from a spray can and is called Molycote G Rapid Spray and is supplied by Dow Corning.

III. Discussions of the Analyses

Appendix 1 contains the derivation of the maximum shear stress in the contact area of a misaligned gear tooth in terms

of the misalignment angle, the tangential load, the pinion pitch diameter, the elastic modulus, and a tooth-shape factor. The maximum shear stresses versus the tooth misalignment are plotted in Fig. 8 for several values of the friction coefficient and for the countertorquing load corresponding to 700 psi. The ordinates of the curves at the left side of the figure pertain to the case of perfect tooth alignment. In order to determine how the calculated maximum shear stresses compare with the shear yield of the gear tooth material, the shear yield value, $\tau_y = 1/\sqrt{3}\,\sigma_y$ from Ref. 7, page 138, will be used. By taking the lower value of 104000 psi tensile yield from Table 1, the lowest value of τ_y becomes 60000 psi or 41370 (10^4) N/m^2. For the case of perfect tooth alignment, the ordinates of the curves at the left edge of Fig. 8 are all well below 60000 psi. The left-edge ordinate values are 14500, 17000, 20000, 22500, and 25500 psi, respectively for the friction coefficients 0.111, 0.20, 0.30, 0.40, and 0.50. It is believed that misalignment angles of more than 0.001 radian seldom occurred. For such a misalignment a friction coefficient of 0.40 would be required to exceed the 60000 psi shear yield. Under wind conditions the shear stresses would of course increase. Equation (A-21) shows that for the case of a misaligned tooth, the maximum shear stress, τ_{max}, varies with the 1/4 power of the tooth load. Hence, for the maximum tooth load at a wind of 22.35 m/sec (50 MPH) the shear stresses would be approximately only $(4)^{0.25} = 1.41$ times as much as indicated by the curves of Fig. 8. But such shear stresses at a misalignment of 0.001 radian would be above the shear yield even at friction coefficients as low as 0.15. These maximum shear stresses at misalignment occur only very close to the end of the gear tooth. Thus, plastic flow has been explained only at the ends of a tooth.

Appendix 2 describes the results of a strain gage test made on two of the bull-gear teeth at DSS 63. From the results of these tests it is concluded that the maximum magnitude of the tooth loading during elevation axis slew is as expected. The vacillating nature of the tooth strain as shown in Fig. 9, however, is not understood. It would appear that, because of the load vacillation, the actual number of loading cycles is approximately twice what was expected.

For the case of no misalignment, Eq. (A-18) shows that the maximum shear stress, τ_{max}, varies with the square root of the load. Therefore, at a wind speed of 22.35 m/sec (50 MPH) the maximum shear stresses would be approximately twice that shown by the ordinates at the left edge of Fig. 8, and these values would be 29000, 34000, 40000, 45000, and 51000 psi, respectively, for the friction coefficients 0.111, 0.20, 0.30, 0.40, and 0.50. None of these is equal to the shear yield, so that plastic flow across the entire width of the gear tooth, as shown in Fig. 5, is not explained.

As stated before, it is believed that the plastic flow damage is caused by the lower but more frequently applied countertorque loading, rather than by the infrequently applied high-wind loading. This opinion is reached by observing that the plastic flow is on all the teeth which come into mesh with the pinions when the elevation axis is slewed through 85°. Figure 4 shows which tooth surfaces show the plastic flow condition. It is estimated that the central teeth undergo 4 slew loadings per day or approximately 1500 per year. After a period of 8 years, 12000 slew loadings would have occurred, and from the strain gage tests which showed a loading vacillation, this could be equivalent to 24000 cyclic loadings during the 8-year period.

It is tempting to try to explain the plastic flow by the phenomenon of strain softening as described in Refs. 5 and 6. Figure 10 is from Ref. 8 and shows that the yield after cyclic loading is approximately half that after monotonic loading. If the shear yield of the bull-gear material were reduced by a factor of two, giving a shear yield of 20685 N/cm^2 (30000 psi), the left-edge ordinates of the curve of Fig. 8 for $\mu = 0.50$ would be getting quite close to the new shear yield. This indeed might be the explanation, but it is difficult to accept because another bull gear on the antenna at DSS 12 has had about the same length of service and is in excellent condition. Its hardness is slightly less than that of the DSS 14 bull gear, and the tooth stress due to countertorquing is somewhat more (Ref. 9) than that of the DSS 14 bull gear. A comparison of these values is set out in Table 2. If strain softening caused the plastic flow at DSS 14, why did not the DSS 12 gear undergo the same softening? At the present time no satisfactory explanation has been offered.

The cylinder of Fig. 11 depicts a roller in contact with a plane surface, represented by the cube. The purpose is to show the direction of the normal Hertz stress, σ_h, and the two at right angles to it, namely, another σ_h and $\sigma_{h/2}$. On the contact surface the frictional force, $\tau_c = \mu\sigma_h$, acts as shown, and this frictional force is the result of gear-tooth sliding. Reference 10 shows that when the friction coefficient exceeds 1/9, the maximum shear is located at the point of contact, but not in the contact plane. The three principal stresses are directed as indicated by σ_{p1}, σ_{p2}, and σ_{p3} and the angles and magnitudes can be calculated by the usual methods of calculating principal directions and stresses, for example, as shown in Ref. 7. Figure 12 shows a multi-view picture of the principal stresses and the maximum shear-stress plane. Notice that when the maximum shear-stress vector is projected onto the contact surface of the gear tooth, it makes a certain angle with the tooth boundary, which appears to be approximately the same as that shown by the ridges of Fig. 5. It seems likely that there might be a relationship between the plastic flow ridges and this

projection of the maximum shear stress. From symmetry, the ridges could have had a mirror-image direction.

IV. Consequences of the Tooth Plastic Flow

It should be emphasized that the plastic flow exists only in the volume of material very near the working surface of the tooth, that is, limited to the region very close to the contact surface. Since both the calculated and measured strains at the tooth root are very small, there is no concern that there will be any catastrophic failure. Since it appears that the corrugated condition of the tooth surfaces is slowly intensifying, there is concern that eventually the pointing accuracy of the antenna will be affected. For example, if the corrugation spacing should be three millimeters and if there were a tendency for a corrugation peak of the pinion to fit into a corrugation valley of the bull gear, the servo drive might not be able to hold the commanded position. The angular pointing error might be approximately three millimeters divided by the radius of the bull gear (3/12650 = 0.000237 radian or 0.013 degree). It is possible that the servo drive could overcome such a situation, nevertheless it is a point of worry.

V. Conclusions and Recommendations

An examination of Table 2 shows that the Hertz stress is higher and the material hardness is lower on the DSS 12 bull gear, which is the one which is in very good condition. The DSS 12 gear-tooth sliding velocity at antenna slew speed is about twice the sliding velocity of the DSS 14 gear at its slew speed. This is because the DSS 12 antenna has a higher angular slew speed. It is conceivable that lubrication is better at the higher sliding velocities.

It is recommended that an attempt be made to determine if the DSS 14 gear teeth have experienced strain softening. Reference 5 states that material softening cannot always be detected by hardness tests. Possibly this can be done by cutting off small material samples and having them examined by metallurgical experts. It is recommended that the consulting services of one or more of the persons experienced in the field of strain softening be obtained. Although the DSS 14 and DSS 12 gear material is nominally the same, it might be that the small actual difference in material composition is significant.

If new gears must be ordered before there is a good understanding of the nature of DSS 14 gear plastic flow, it is recommended that both the bull gears and pinions be made harder. If strain softening is limited to some certain percentage of the original yield strength, then a sufficient increase in the original yield strength could prevent the plastic flow. Gear manufacturers have stated that it is feasible to cut through-hardened gears having a Brinell hardness of 320 to 360. Greater hardnesses near the surface could be obtained by flame or induction hardening. The hardness of pinions should be appreciably more than that of the gears.

Two or more gear consulting engineers have regretted that a better lubricant is not being used, yet they have been unable to recommend a better one for the existing environmental conditions. There are lubrication specialists who concoct special lubricants for special situations. It is also recommended that the services of such a specialist be obtained.

Table 1. Gear Specifications

	Bull Gear	Pinion
Tooth Type	Spur	Spur
Circular Pitch, mm	88.90	88.90
Pitch Diameter, m	25.298	0.4527
Outside Diameter, m	25.341	0.5235
Addendum, mm	21.209	35.382
Whole Depth, mm	61.036	63.665
Root Diameter, m	25.219	0.3962
Backlash with Mate, mm	0.635 to 1.016	0.635 to 1.016
Material	4140 Steel	4140 Steel
Brinell Hardness Range	245 to 285	285 to 325
Tensile Yield (psi)[(a)]	104000 to 118000	118000 to 140000
JPL Drawing Number	9436786	9435055
Pressure Angle	25°	25°
Contact Ratio 1.44		

[a]Tensile yield stresses, corresponding to Brinell values, are from Reference 11.

Table 2. Comparison of three antenna bull gear tooth stresses, hardnesses, and condition

Antenna	Lubricant	Gear tooth load from countertorque N (lb)	Nominal Hertz stress at full tooth contact N/cm^2 (psi)	Gear material steel	Brinell hardness range	Max. sliding velocity of tooth at max. slew speed cm/sec (inch/sec)	Condition
64-m DSS 14	Molycote	69144 (15545)	33360 (48385)	4140	285 245	1.89 (0.745)	Plastic flow damage
26-m DSS 12	Molycote	19046 (4282)	43000 (62368)	4140	260 220	2.95 (1.161)	Excellent
34-m DSS 15	Molycote	42548 (9568)	41955 (60850)	4340	320 280		New

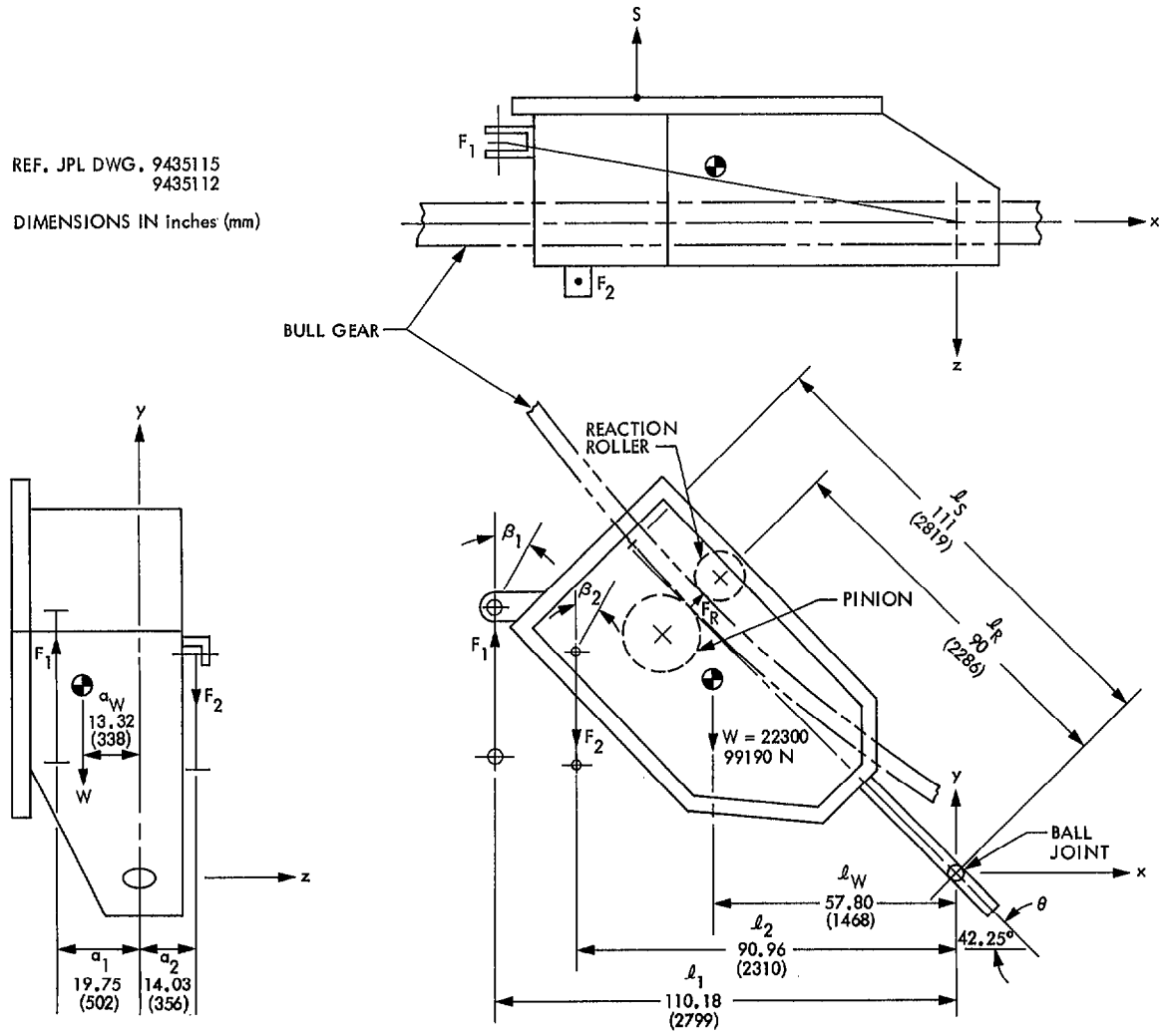

Fig. 1. Upper elevation drive gear box no. 2

REF. JPL DWG. 9435115
9435110

DIMENSIONS IN inches (mm)

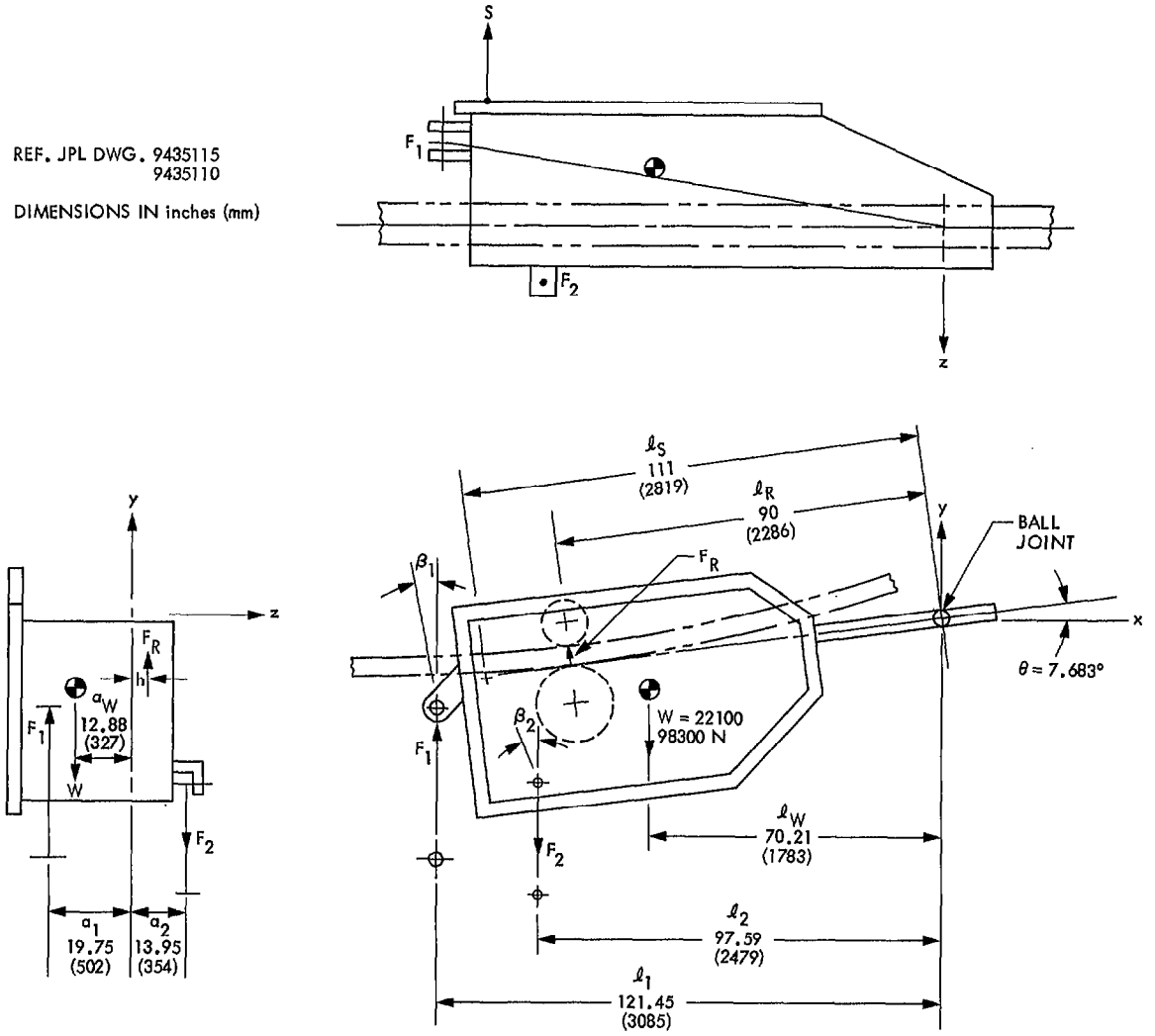

Fig. 2. Lower elevation drive gear box no. 3

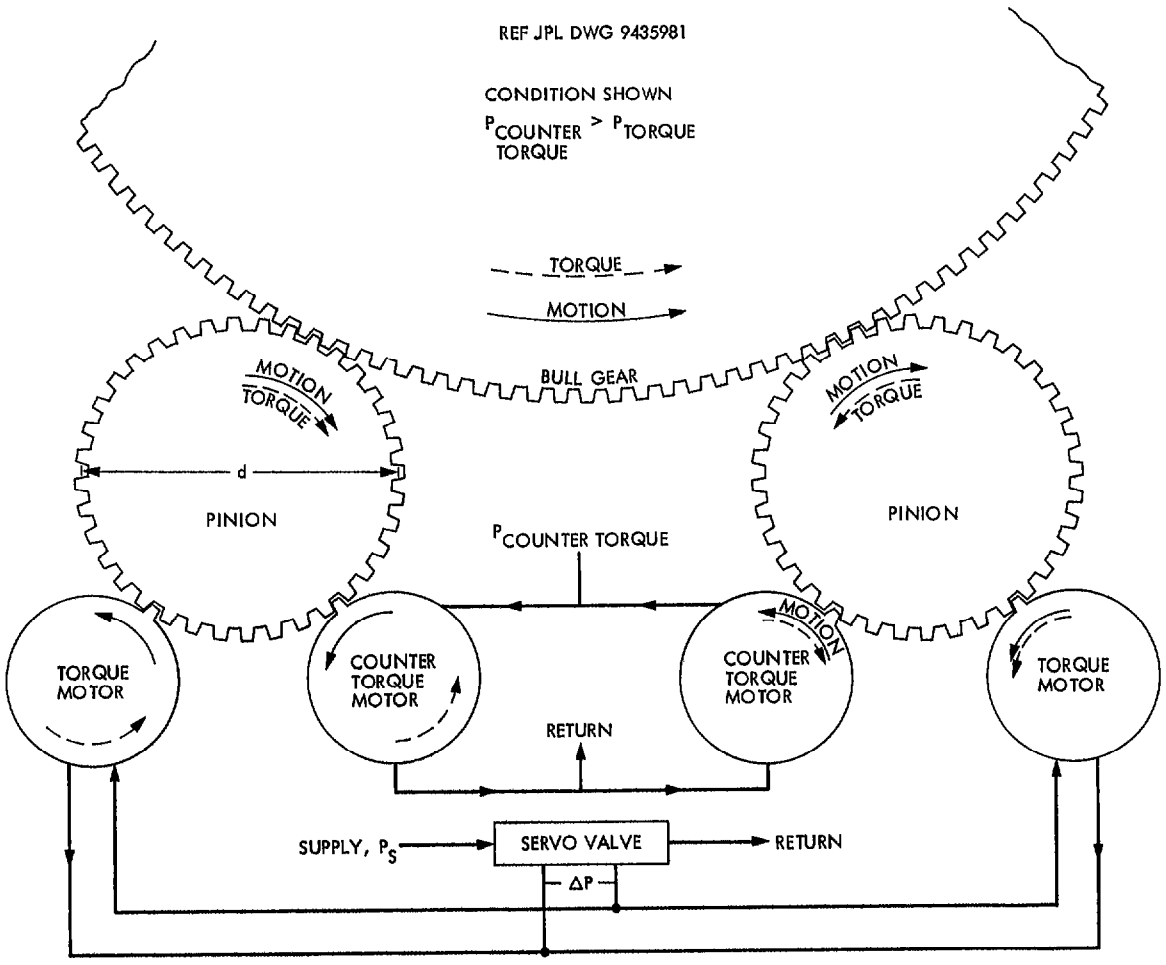

Fig. 3. Schematic of bull gear, pinions, hydraulic motors, and servo valve

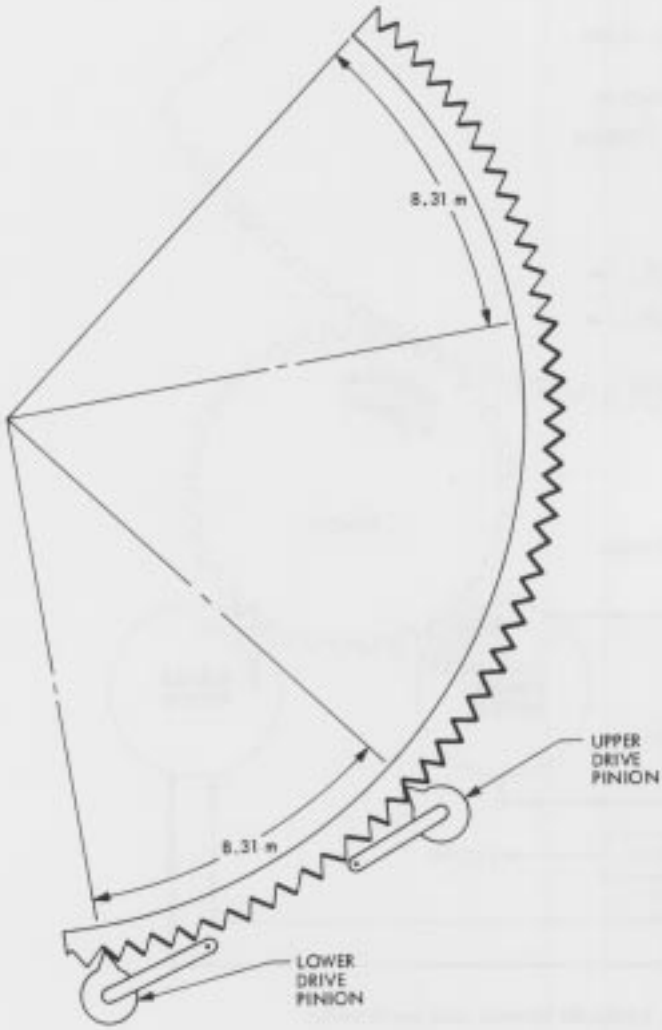

Fig. 4. Schematic of bull gear showing, by heavy lines, the tooth surfaces subjected to countertorque loading

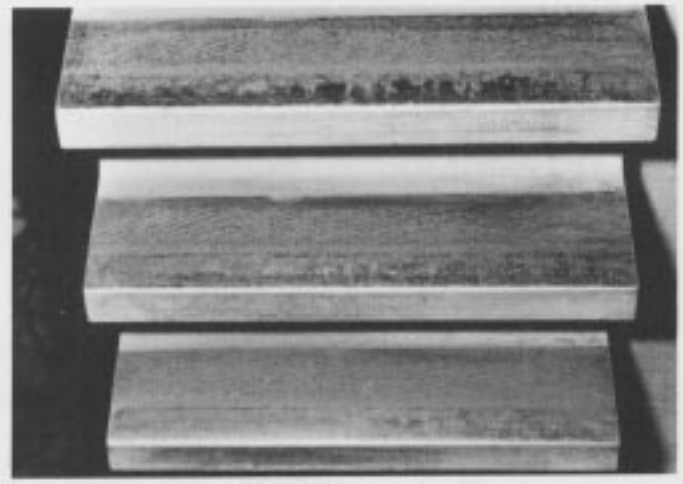

Fig. 5. Plastic flow across entire width of bull gear tooth

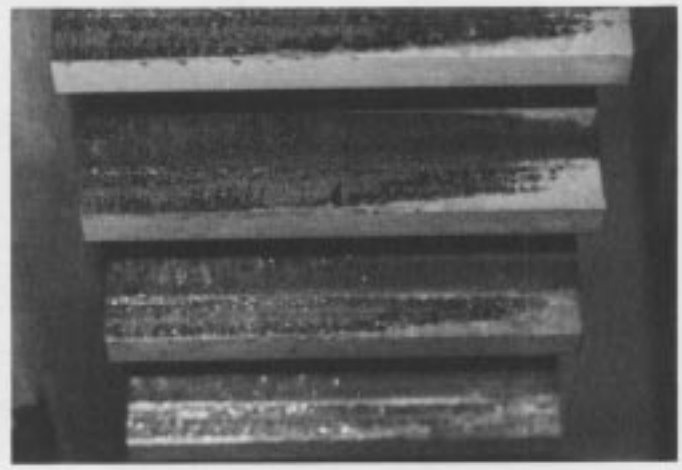

Fig. 6. Change in direction of corrugation pattern across pitch line

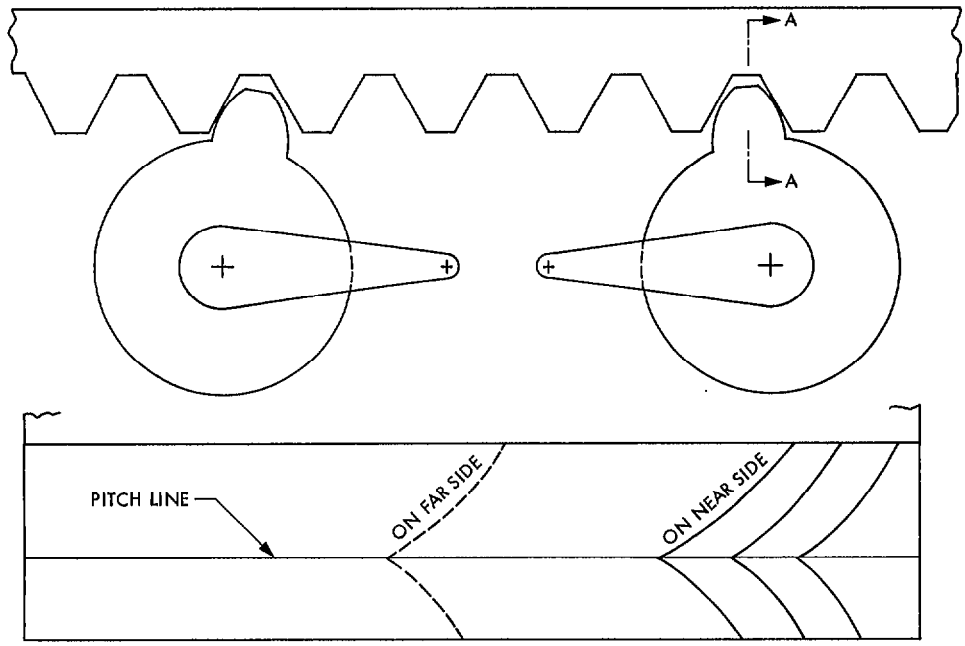

VIEW A-A

Fig. 7. Schematic of tooth ridge pattern

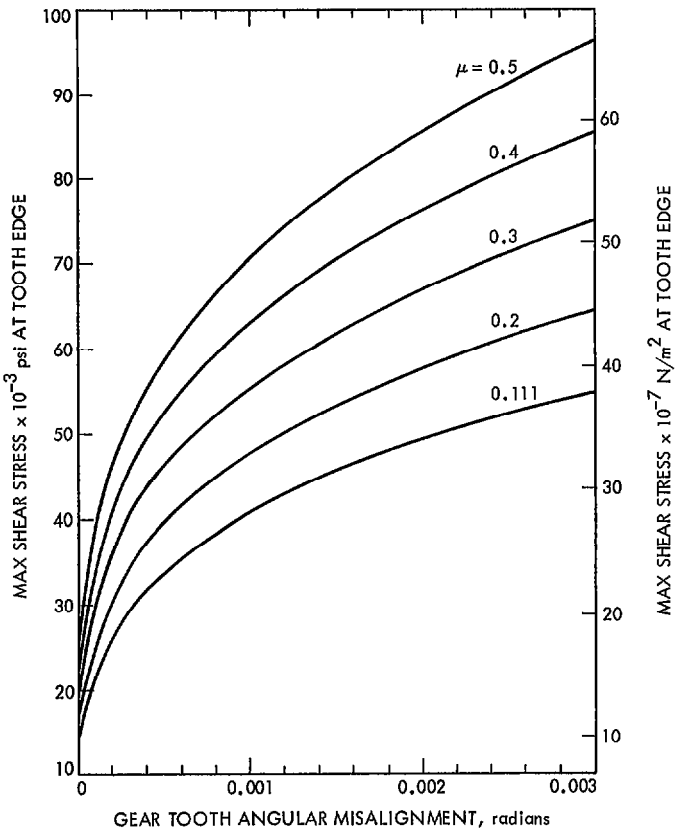

Fig. 8. Maximum shear stress versus tooth misalignment

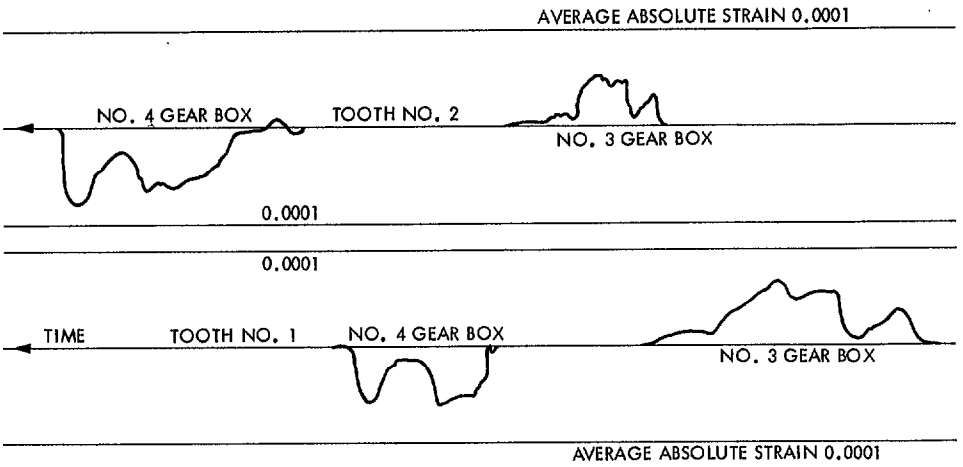

Fig. 9. Average absolute strain of gages on two different teeth of a bull gear, measured at DSS 63, elevation axis speed 0.0042 deg/sec

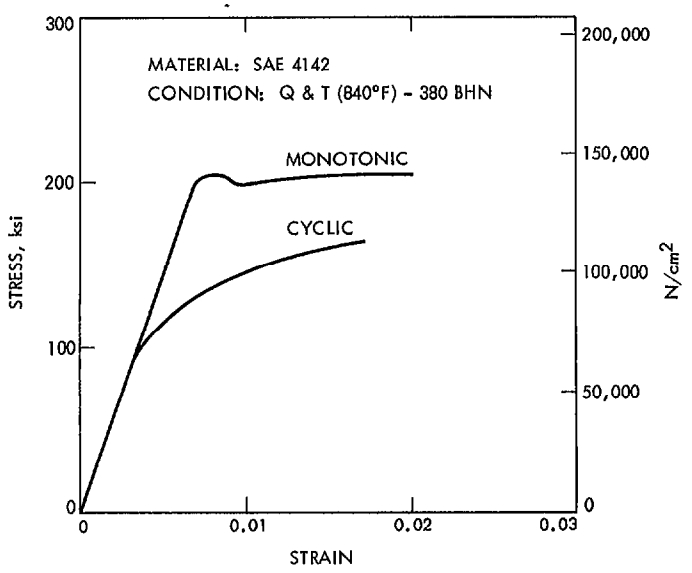

Fig. 10. Stress strain curve for material which has strain softened under cyclic loading

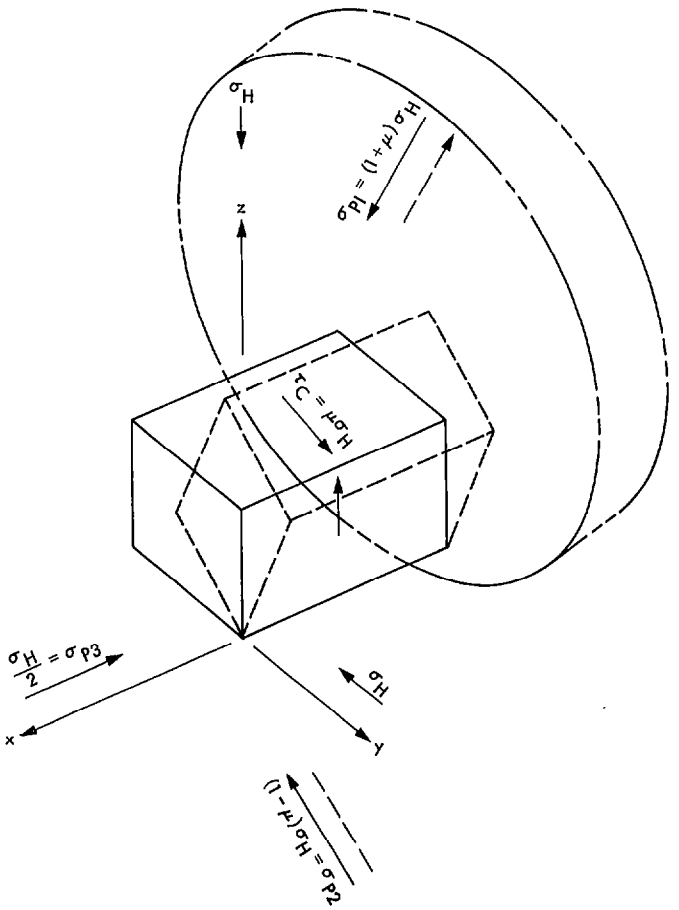

Fig. 11. Orientation of principal stresses σ_{P1}, σ_{P2}, σ_{P3} with respect to x-axis, which is parallel to roller axis

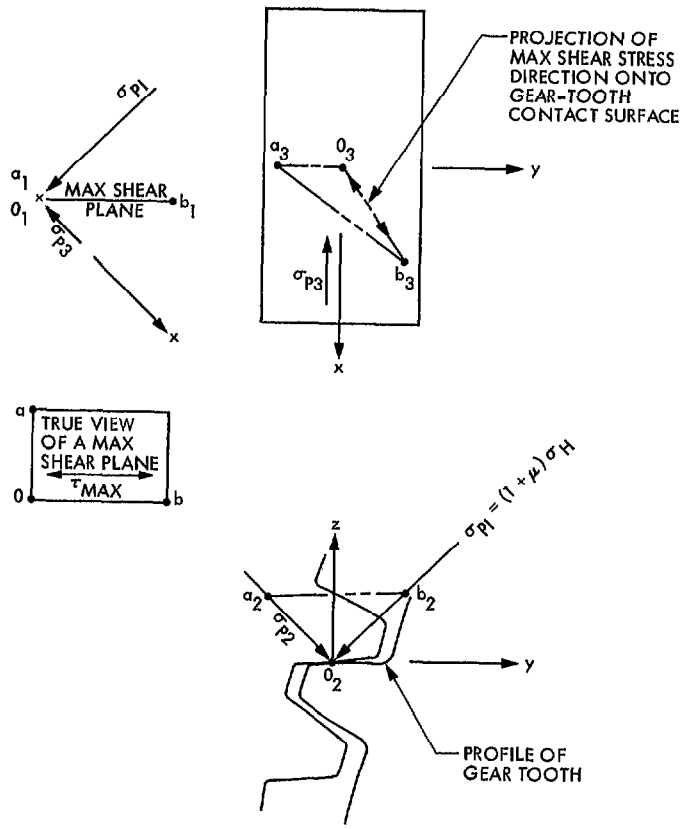

Fig. 12. Multiple view orientation of maximum shear direction

Appendix A

Figure A-1 depicts the contact between the teeth of a misaligned gear set. When contact first occurs at the right-hand edge, the clearance at the left edge is γ. As the force between the teeth increases, the contact becomes a flat surface which bisects the angle θ formed by the dashed lines of the figure. At equilibrium the length of contact is h. Let the origin of x be where contact begins. From Fig. A-1, the following relationships may be obtained:

$$Y = Y_{MAX}\frac{x}{h} = \frac{\delta_2}{2h}x \tag{A-1}$$

$$\delta_1 + \delta_2 = \gamma \tag{A-2}$$

$$\delta_1 = \frac{\ell - h}{h}\delta_2 \tag{A-3}$$

$$\delta_2 = \frac{h}{\ell}\gamma \tag{A-4}$$

$$\theta = \frac{\delta_2}{h} \tag{A-5}$$

Substitute (A-5) into (A-1) and obtain:

$$Y = \frac{\theta}{2}x \tag{A-6}$$

From Ref. 13, the following expression for the deflection, Y_u, of a cylindrical roller of length ℓ, when pressed against a flat plate of infinite extension is:

$$Y_u = 2.54\frac{P^{.9}}{E^{.9}\ell^{.8}} \tag{A-7}$$

where

P is the total force between the plate and the roller

E is the common elastic modulus of the plate and the roller

Y_u is the deflection of the center of the roller

The deflection Y_u is caused by local deformation in the roller and in the plate. If these two components of deflection are assumed to be equal, then the local deflection of either is half that given by (A-7) namely

$$Y_u = 1.27\frac{P^{.9}}{E^{.9}\ell^{.8}} \tag{A-8}$$

Solving for P there is obtained:

$$P = \left(\frac{Y}{1.27}\right)^{10/9} E\,\ell^{8/9} \tag{A-9}$$

If it is assumed that the load per unit length, w, can be approximated by dividing (A-9) by ℓ, then:

$$w = \left(\frac{Y}{1.27}\right)^{10/9}\frac{E}{\ell^{1/9}} \tag{A-10}$$

Substituting (A-6) into (A-10) and letting $\ell = h$, yields:

$$w = \left(\frac{\theta x}{2.54}\right)^{10/9}\frac{E}{h^{1/9}} \tag{A-11}$$

The total tangential force acting on the gear tooth, F, must be equal to the integral of (A-11) between the limits h and zero.

$$F = \int_0^h w\,dx = \left(\frac{\theta}{2.54}\right)^{10/9}\frac{E}{h^{1/9}}\int_0^h x^{10/9}\,dx$$

$$= 0.168\,E\theta^{10/9}\,h^2 \tag{A-12}$$

Solve (A-12) for h and obtain:

$$h = \left[\frac{F}{0.168\,E\theta^{10/9}}\right]^{1/2} \tag{A-13}$$

Substitute (A-13) into (A-11), let $x = h$ and obtain w_{MAX}:

$$w_{MAX} = 0.8656\,E^{1/2}\,F^{1/2}\,\theta^{5/9} \tag{A-14}$$

Equation (A-14) expresses the maximum load per unit length in terms of the elastic modulus, the gear tangential load, and the angular misalignment.

The task now is to express w_{MAX} in terms of the maximum stress and the gear-tooth dimensions.

From Ref. 3 the Hertz stress, σ_H, for the case of normal stresses only at the contact, is:

$$\sigma_{H0} = 0.798\sqrt{\frac{wE\left(1+\frac{1}{\rho}\right)}{d(1-\nu^2)\sin 2\phi}} \qquad \text{(A-15)}$$

where

ρ is the gear-to-pinion diameter ratio

ν is Poisson's ratio

d is the pinion pitch diameter

ϕ is the pressure angle of the involute gear

The maximum shear stress, τ_{0MAX}, for the condition of only normal stresses at the tooth contact, exists beneath the contact surface, and its magnitude is:

$$\tau_{0MAX} = 0.304\,\sigma_{H0} \qquad \text{(A-16)}$$

Reference 10 shows that if frictional forces exist at the contact surface, the location of the maximum shear stress is closer to the surface, and if the friction coefficient is greater than 1/9, the maximum shear stress is at the surface. By using the Ref. 10 equations for the stress components, and letting Poisson's ratio be 1/4, the following expression for the maximum shear stress, τ_{MAX}, can be derived:

$$\tau_{MAX} = [0.575\,\mu + 0.238]\,\sigma_o, \text{ for } \mu > \frac{1}{9} \qquad \text{(A-17)}$$

where μ is the friction coefficient.

Substitute (A-15) into (A-17) and obtain:

$$\tau_{MAX} = (0.459\,\mu + 0.190)\sqrt{\frac{wE\left(1+\frac{1}{\rho}\right)}{d(1-\nu^2)\sin 2\phi}} \qquad \text{(A-18)}$$

Let ν be 1/4, and C be

$$\frac{1+\frac{1}{\rho}}{\sin 2\phi},$$

then (A-18) becomes:

$$\tau_{MAX} = (0.473\,\mu + 0.196)\sqrt{\frac{wEC}{d}}, \quad \mu > \frac{1}{9} \qquad \text{(A-19)}$$

Solve (A-19) for w and obtain:

$$w = \left(\frac{\tau_{MAX}}{0.473\,\mu + 0.196}\right)^2 \frac{d}{EC} \qquad \text{(A-20)}$$

Equate (A-20) to (A-14), solve for τ_{MAX}, and obtain:

$$\tau_{MAX} = \frac{(0.44\,\mu + 0.182)\,C^{1/2}\,E^{3/4}\,F^{1/4}\,\theta^{5/18}}{d^{1/2}} \qquad \text{(A-21)}$$

Estimates of maximum shear stress can be made using the following equations.

If the friction coefficient μ is less than 1/9 and the gear misalignment is zero use equations (A-15) and (A-16) to obtain:

$$\tau_{MAX} = 0.241\sqrt{\frac{wEC}{d(1-\nu^2)}} \qquad \text{(A-22)}$$

If the friction coefficient is less than 1/9 and there is a gear-tooth angular misalignment θ,

$$0.241\sqrt{\frac{wEC}{d(1-\nu^2)}} < \tau_{MAX} \leqslant 0.232\,\frac{C^{1/2}\,E^{3/4}\,F^{1/4}\,\theta^{5/18}}{d^{1/2}} \qquad \text{(A-23)}$$

If the friction coefficient is greater than 1/9 and the gear misalignment is zero, then:

$$\tau_{MAX} = (0.473\,\mu + 0.196)\sqrt{\frac{wEC}{d}} \qquad \text{(A-24)}$$

If the friction coefficient is greater than 1/9 and there is a gear-tooth angular misalignment θ,

$$(0.473\,\mu + 0.196)\sqrt{\frac{wEC}{d}} < \tau_{MAX}$$

$$\leqslant (0.44\,\mu + 0.182)\,\frac{C^{1/2}\,E^{3/4}\,F^{1/4}\,\theta^{5/18}}{d^{1/2}} \qquad \text{(A-25)}$$

These maximum shear stresses are plotted in Fig. 8 for the following values of the parameters which pertain to the 64-m antenna elevation drive gears.

C = 1.329, E = 29,000,000 psi or 19,994 716 (10^4) N/m^2

F = 15,545 lb or 69,144 N

d = 17.825 inches or 0.453 m

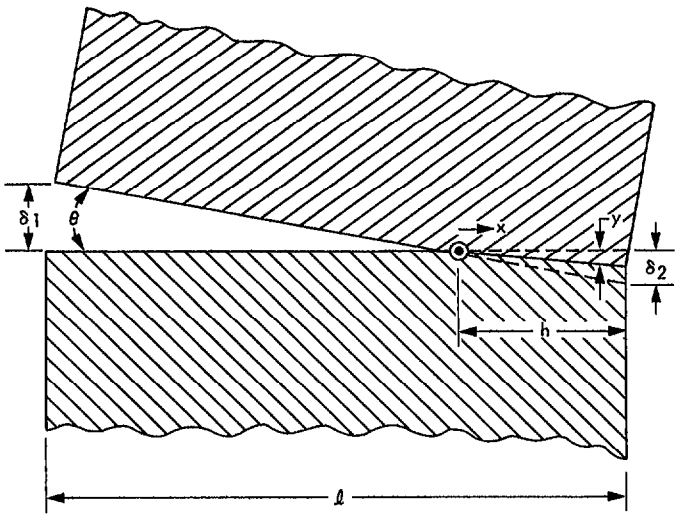

Fig. A-1. Geometry of misaligned gear teeth

Appendix B

Measurement of Bull Gear Tooth Bending Strain

In order to verify that the gear-tooth loading from countertorque is close to the calculated value, two bull-gear teeth were instrumented with foil strain gages so that the average absolute strain value could be measured. The locations of the gages on the ends of one tooth, as well as the bridge circuitry, are shown in Fig. B-1. The tests were conducted in April 1984 at DSS 63 because DSS 14 was undergoing extensive repair at the time. Calculated values should be fairly accurate, but in view of the plastic flow which has developed on the tooth surfaces it was wondered if there might be some dynamic effect which substantially increased the expected strain values. To determine if the tooth loading was speed dependent, the tests were run at various slew speeds and at a typical tracking speed.

I. Installation of the Strain Gages and Recording Equipment

(1) The strain gages were mounted on the edges of a tooth as shown in Fig. B-1. The four gages on one tooth constituted the resistances of the four legs of a Wheatstone bridge; hence, all the gages were active, thereby producing the maximum sensitivity.

(2) Two separate teeth were instrumented with sets of four gages in order to improve the reliability of obtaining good data.

(3) The teeth on which the gages were placed were located sufficiently far from the gear ends so that the gaged teeth meshed with both drive pinions at full slew speed.

(4) The gages were the foil type, having gage factors of approximately 2 and resistances of 350 ohms. The gages used were obtained from Measurements Group, Inc., of Raleigh, N.C., and are model number EA-06-125 AC-350 Option W3. The cement used was M Bond 200. The bridge input voltage was 10 volts DC.

(5) The ancillary equipment used consisted of a bridge balance supply unit, an amplifier, and a signal recorder having at least a 40-Hz response.

A. Conditions of Tests

The tests were conducted under the following conditions:

(1) The wind was less than 4.47 m/second.

(2) The countertorque pressure was 483×10^4 N/m^2 (700 psi).

(3) Both instrumented teeth were recorded while being driven past both drive pinions at an angular speed of 0.0042 degrees per second.

(4) Both instrumented teeth were recorded while being driven past both drive pinions at 0.0042 degrees per second, in the direction opposite to that of step 3.

(5) Both instrumented teeth were recorded while being driven past both pinions at the slew speed of 0.20 degree per second.

(6) Both instrumented teeth were recorded while being driven past both pinions at the slew speed of 0.20 degree per second, in the direction opposite to that of step 5.

(7) Both instrumented teeth were recorded while being driven past both pinions at the slew speed of 0.10 degree per second.

(8) Both instrumented teeth were recorded while being driven past both pinions at the slew speed of 0.10 degree per second, in the direction opposite to that of step 7.

B. Estimation of the Strain at the Gage

The tangential force between a countertorquing pinion and the bull gear, F_T, is given by the following equation (see Fig. 3):

$$F_T = \frac{2pDR\eta}{d} \tag{B-1}$$

where

p is the pressure to the hydraulic countertorquing motor

D is the hydraulic-motor displacement per radian

R is the gear-box ratio

η is the gear-box efficiency

d is the gear-box output pinion pitch diameter

For the 64-m antenna, the tangential force is:

$$F_T = \frac{2\,(700)(0.385)514(0.92)}{17.82} = 14{,}300 \text{ lb } (63{,}600 \text{ N}) \tag{B-2}$$

The bending stress, σ_b, at the tooth root per the Lewis formula [Ref. 3] is:

$$\sigma_b = \frac{F_T}{aLS} = \frac{14{,}300}{3.5(9.75)0.15} = 2430 \text{ psi } (1675 \text{ N/cm}^2) \quad \text{(B-3)}$$

where

a is the circular pitch

L is the tooth width

S is the form factor

The estimated stress at the gages, σ_G, is less than σ_b because the gages are closer to the neutral axis, and is:

$$\sigma_G = 2430 \frac{1.35}{1.50} = 2187 \text{ psi } (1508 \text{ N/cm}^2) \quad \text{(B-4)}$$

The strain at the gages, ϵ_G, is:

$$\epsilon_G = \frac{\sigma_G}{E} = \frac{2187}{29{,}000{,}000} = 0.0000754 \quad \text{(B-5)}$$

The voltage-output-to-voltage-input ratio of the gage circuitry shown in Fig. B-1 is:

$$\frac{V_o}{V_{IN}} = \frac{\Delta r}{r} = f\epsilon \quad \text{(B-6)}$$

where f is the defined gage factor.

The calibration strain, ϵ_c, was obtained by shunting across one leg of the bridge with a 811,000-ohm resistor. The calibration strain was:

$$\epsilon_c = \frac{r}{4(r+R)f} = \frac{350}{4(350+811{,}000)2} = 0.0000539 \quad \text{(B-7)}$$

By comparing the recorded bridge output voltage signals to the calibration signal, which corresponds to a strain of 0.0000539, the desired strains, ϵ_G, were obtained:

$$\epsilon_G = \epsilon_c \times \frac{\text{Recorded Signal Amplitude}}{\text{Recorded Calibration Amplitude}} \quad \text{(B-8)}$$

The maximum strain, ϵ_G, was found to be 0.0000772, which may be compared with the estimated value of 0.0000754 from Eq. (B-5). Therefore, it is clear that none of the elevation axis speeds tested caused any unexpected high gear-tooth forces. Traces from the actual strip chart are shown in Fig. 9. Although the maximum strain values are close to the predicted ones, the vacillating characteristics of the curves is not understood.

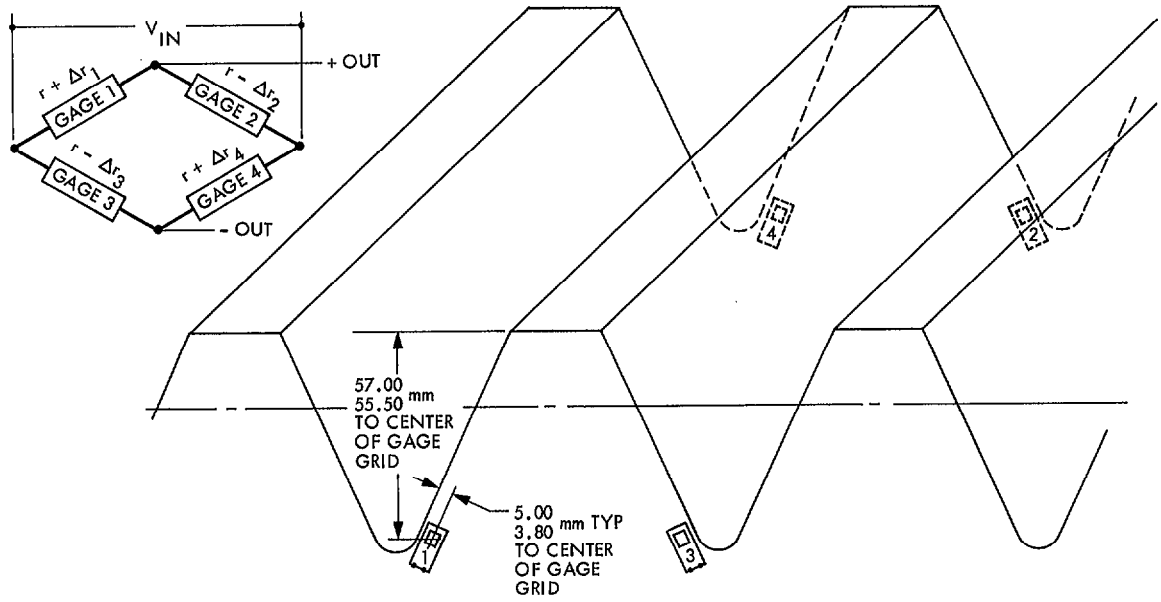

Fig. B-1. Location of strain gages on elevation drive bull gear and strain gage bridge

Appendix C

Estimation of Nominal Hertz Stress in the DSS12 Declination Bull Gear

The antenna at DSS 12, before its conversion to a 34-m antenna with electric drives, was a 26-m antenna with hydraulic drives incorporating countertorquing, which served to eliminate backlash. Thus, its drives were similar to those of the DSS 14 antenna. Reference 9 shows that a differential pressure of 300 psi was used on the two drive motors, so that for a zero wind condition the tangential force on the bull-gear tooth can be calculated by Eq. (B-1), obtaining:

$$F_T = \frac{2(\Delta p)DR\eta}{d} = \frac{2(300)(0.232)(285)0.80}{6.50} = 4882 \text{ lb} \tag{C-1}$$

From Eq. (A-15) the nominal Hertz stress, σ_{H0}, at full tooth contact is:

$$\sigma_{H0_{12}} = 0.798\sqrt{\frac{wE\left(1+\frac{1}{\rho}\right)}{d(1-\nu^2)\sin 2\phi}}$$

$$= 0.798\sqrt{\frac{814(29)10^6\left(1+\frac{1}{73.8}\right)}{6.5\,(1-0.25^2)\sin 40^\circ}} = 62{,}368 \text{ psi} \tag{C-2}$$

where $w = F/\ell = 4882/6 = 814$ lb/inch.

The corresponding stress for the DSS 14 elevation bull gear is:

$$\sigma_{H0_{14}} = 0.798\sqrt{\frac{15545\,(29)\,10^6\left(1+\frac{1}{56}\right)}{9.75(17.825)(1-0.25^2)\sin 50^\circ}}$$

$$= 48385 \text{ psi} \tag{C-3}$$

Acknowledgment

Drs. C. Chian and C. Hsieh of JPL directed our attention to the phenomenon of strain softening under cyclic loading and supplied a great deal of information on the subject.

References

1. McGinness, H., Characteristics of the Elevation Drive Suspension of the 64m Antennas, *TDA Progress Report 42-80*, March, 1985, pp. 146-175, Jet Propulsion Laboratory, Pasadena, California.
2. McGinness, H., *The Effects of Wind Loading on the Bearings and Drives of a 64m and 72m Diameter Antenna*, unpublished, Reorder number 84-2, Jet Propulsion Laboratory, Pasadena, California, May, 1984.
3. Buckingham, E., *Analytical Mechanics of Gears*, McGraw-Hill, First Edition, 1949.
4. *AGMA Standard, Nomenclature of Gear Tooth Failure Modes*, American Gear Manufacturers Association, August, 1980, p. 16.
5. Sandor, I., *Fundamentals of Cyclic Stress and Strain*, University of Wisconsin Press, 1972.
6. Raske and Morrow, *Mechanics of Materials in Low Cycle Fatigue Testing*, Manual on Low Cycle Fatigue Testing, ASTM STP 465, American Society for Testing Materials, 1969.
7. Timoshenko, S., *Theory of Elasticity*, McGraw-Hill, First Edition, 1934.
8. Landgraph, Mitchell, and LaPointe, *Montonic and Cyclic Properties of Engineering Materials*, Ford, 1972.
9. Menninger, F., *26m Antenna HA-dec Counter Torque Modifications*, Technical Report 32-1526, Vol. III, Jet Propulsion Laboratory, Pasadena, California, March, 1971.
10. Smith and Liu, "Stresses Due to Tangential and Normal Loads on an Elastic Solid with Applications to Some Contact Stress Problems," *Journal of Applied Mechanics*, June, 1953.
11. *Properties of Frequently Used Carbon and Alloy Steels*, Booklet 211, Bethlehem Steel Co., 1946, p. 60.
12. Levy, R. and H. McGinness, *Wind Power Prediction Model*, Technical Memorandum 33-802, Jet Propulsion Laboratory, Pasadena, California, 1976.
13. Palmgren, A., *Ball and Roller Bearing Engineering*, SKF Industries, Third Edition, 1959.